

PREPARED FOR SUBMISSION TO JCAP

The role of the *eROSITA* all-sky survey in searches for sterile neutrino dark matter

Fabio Zandanel, Christoph Weniger, and Shin'ichiro Ando

GRAPPA Institute, University of Amsterdam, 1098 XH Amsterdam, The Netherlands

E-mail: f.zandanel@uva.nl, c.weniger@uva.nl, s.ando@uva.nl

Abstract. We investigate for the first time the potential of angular auto- and cross-correlation power spectra in identifying sterile neutrino dark matter in the cosmic X-ray background. We take as reference the performance of the soon-to-be-launched *eROSITA* satellite. The main astrophysical background sources against sterile neutrino decays are active galactic nuclei, galaxies powered by X-ray binaries, and clusters of galaxies. While sterile neutrino decays are always subdominant in the auto-correlation power spectra, they can be efficiently enhanced when cross-correlating with tracers of the dark matter distribution such as galaxies in the 2MASS catalogues. We show that the planned four-years *eROSITA* all-sky survey will provide a large enough photon statistics to potentially yield very stringent constraints on the decay lifetime, enabling to firmly test the recently claimed 3.56-keV X-ray line found towards several clusters and galaxies and its decaying dark matter interpretation. However, we also show that in order to fully exploit the potential of *eROSITA* for dark matter searches, it is vital to overcome the shot-noise limitations inherent to galaxy catalogues as tracers for the dark matter distribution.

Contents

1	Introduction	1
2	Signal and backgrounds in X-ray searches for sterile neutrinos	3
2.1	Sterile neutrino dark matter	3
2.2	Active galactic nuclei	4
2.3	Galaxies	6
2.4	Clusters of galaxies	6
3	Auto-correlations of the angular power spectrum	8
4	Cross correlations with the 2MASS galaxy catalogues	11
5	Detectability and projected limits	14
5.1	Statistical method	15
5.2	Projected limits	16
6	Conclusions	18
A	Treatment of correlated statistical uncertainties	20
B	Auto- and cross-correlation power spectra	21

1 Introduction

Revealing the non-gravitational nature of dark matter particles is one of the most important goals of modern astrophysics and cosmology. Even though weakly interacting massive particles (WIMPs) are among the most popular and well-motivated candidates [1, 2], so far no established signature thereof has been found at colliders, direct, or indirect searches. This urges the investigation of alternative possibilities. Sterile neutrinos with keV masses are well-known and well-motivated candidates for dark matter [3–6]. Observationally, keV-mass sterile neutrinos are interesting as they behave as warm dark matter (WDM). This can potentially mitigate some of the small-scales problems of the cold dark matter (CDM) scenario, e.g., the so called missing satellite and too-big-to-fail problems, or alternatively provide indirect evidence for sterile neutrino dark matter (see, e.g., [7]).

Sterile neutrinos are spin-1/2 singlets under the Standard Model gauge group, and can decay into photon-neutrino pairs, $\nu_s \rightarrow \gamma\nu$. A clear smoking gun signal for sterile neutrino dark matter would be the detection of monochromatic photons at half of the dark matter mass. The corresponding decay rate is proportional to the mixing angle θ^2 between active and sterile neutrinos, and is given by [5, 8]

$$\Gamma_{\nu_s} \simeq (7.2 \times 10^{29} \text{ s})^{-1} \left(\frac{\sin^2 2\theta}{10^{-8}} \right) \left(\frac{m_{\nu_s}}{1 \text{ keV}} \right)^5, \quad (1.1)$$

where m_{ν_s} is the sterile neutrino mass.

Monochromatic lines from sterile neutrinos have been searched for in various different targets, such as nearby galaxies and galaxy clusters [9–14]. Recently, there have been claims of the detection of an unidentified 3.56-keV line from a stacked sample of galaxy clusters [15], and from Andromeda and the Perseus cluster [16], with a subsequent number of works on the issue, some of which confirmed the claim [17–20] and some not [21–27]. This is an ongoing debate that deserves further investigation (see, e.g., [28]).

One modern and very promising approach to indirect dark matter searches with photons at all wavelengths is the cross-correlations between the electromagnetic signal and tracers of the dark matter distribution [29, 30]. Up to now, these searches were mostly related to dark matter annihilation in the gamma-ray regime, with few studies also on decaying dark matter [29, 31, 32]. The main reason being that the focus of indirect dark matter searches so far has been mainly on WIMPs and their gamma-ray annihilation and decay products. However, as already mentioned, the lack of any strong evidence for WIMPs have recently broadened the interest of the community, particularly after the 3.56-keV line claim and its sterile neutrino dark matter interpretation.

Cross-correlation searches aim at the dark matter signal coming from cosmological distances, and have the advantage of exploiting simultaneously spatial and spectral information from the full sky. As tracers for dark matter in the local Universe, galaxy catalogues [30] and cosmic shear (weak gravitational lensing) [29, 33] proved to be very promising. Additionally, with a tomographic approach one can further exploit the redshift information, which allows a better discrimination between various astrophysical and dark matter related photon sources [31, 34, 35]. The power of such cross-correlation searches manifested recently in the first discovery of cross-correlations of the *Fermi*-Large Area Telescope gamma-ray sky with the CMB [36] and galaxy catalogues [37], with important implications for WIMP dark matter searches studied in Refs. [38, 39]. A recent exhaustive review about the gamma-ray emission from cosmological distances, and the potential of cross-correlation studies, can be found in Ref. [40] (see also Ref. [41] for a detailed discussion about the expected WIMP dark matter signal).

In the present paper, we investigate for the first time the potential of an angular power spectrum analysis of the cosmic X-ray background (CXB) in identifying sterile neutrino dark matter. The methods that we present are very general and can be used for all scenarios with decaying dark matter. We will show that the auto-correlation power spectrum of X-ray emission from sterile neutrinos is completely dominated by background sources, in particular by active galactic nuclei (AGNs) and clusters of galaxies. However, as we will demonstrate, the *cross-correlation* with tracers of the dark matter distribution in the Universe, like large galaxy catalogues, can greatly enhance the sensitivity towards a sterile neutrino contribution to the X-ray flux, and hence can be a sensitive probe of dark matter signals.

For the purpose of such a CXB analysis, a deep and (nearly) all-sky survey with good energy and angular resolution is a fundamental requirement. The last X-ray all-sky survey has been performed by ROSAT (e.g., [42]). Current X-ray instruments such as XMM-*Newton* (e.g., [43]) and *Chandra* (e.g., [44]) have impressive performances and achievements. However, they only operate in pointed observations. The next X-ray all-sky survey will be performed by *eROSITA* [45], whose launch is scheduled for 2016, with a set of 6-month full-sky observations up to four years. Therefore, *eROSITA* will be the reference for our predictions.

As an exemplary (and readily available) tracer for the nearby dark matter distribution in the local Universe, we will adopt the 2MASS galaxy catalogue [46]. It provides a nearly

complete information on the distribution of galaxies up to $z \approx 0.1$, with a sky coverage of 91%. We will discuss also the potential ultimate reach of our method when other tracers are adopted.

The paper is organised as follows. In section 2 we will discuss in detail the different background and the signal contributions to the CXB. Their auto-correlation power spectrum is discussed in section 3, whereas the cross-correlation power spectrum with tracers of dark matter is discussed in section 4. In section 5 we present our projected sensitivity for future instruments. Eventually, in section 6, we present our conclusions.

If not specified otherwise, we adopt a halo mass M_Δ defined with respect to a density that is $\Delta = 200$ times the *critical* density of the Universe at redshift z . Throughout the paper, we assume a standard Λ CDM cosmology with the parameters $\Omega_\Lambda = 0.73$, $\Omega_m = 0.27$, $\Omega_b = 0.05$, $\Omega_{\text{dm}} = 0.22$, and $H_0 = 100 h \text{ km s}^{-1} \text{ Mpc}^{-1}$ with $h = 0.7$.

2 Signal and backgrounds in X-ray searches for sterile neutrinos

In the following three sections, we will discuss and characterise the mean intensity of a sterile neutrino dark matter signal and of the most relevant background components. These backgrounds are fluxes from AGNs, X-ray binaries hosted in galaxies, and emission from clusters of galaxies.

2.1 Sterile neutrino dark matter

The intensity of photons from sterile neutrino decay into $\gamma\nu$ final states along the direction \mathbf{n} , defined as a number of photons received per unit area, time, solid angle, and energy range, is given by¹

$$I_{\nu_s}(E, \chi \mathbf{n}) = \frac{\Gamma_{\nu_s}}{4\pi m_{\nu_s}} \int_0^\infty \frac{dz}{H(z)(1+z)^3} \rho_{\nu_s}(z, \chi \mathbf{n}) \delta_D \left[(1+z)E - \frac{m_{\nu_s}}{2} \right], \quad (2.1)$$

where δ_D is the Dirac delta function, $H(z) = H_0 \sqrt{\Omega_m(1+z)^3 + \Omega_\Lambda}$ is the Hubble parameter as function of redshift z , $\rho_{\nu_s}(z, \chi \mathbf{n}) = \rho_{\text{dm}}(z, \chi \mathbf{n})$ denotes the mass density of sterile neutrino dark matter in the direction \mathbf{n} at a distance z , and χ is the co-moving distance.

We will first evaluate the mean intensity of extragalactic sterile neutrino dark matter and hence the overall contribution to the CXB. We note that adopting the ensemble average yields $\langle \rho_{\nu_s}(z, \chi \mathbf{n}) \rangle = (1+z)^3 \Omega_{\nu_s} \rho_c = (1+z)^3 \Omega_{\text{dm}} \rho_c$, where ρ_c is the present critical density of the Universe. Therefore, after taking the ensemble average of Eq. (2.1), and convolving with a normal distribution in energy in order to represent the finite energy resolution of an X-ray telescope, the mean intensity due to the sterile neutrino decay is given by

$$I_{\nu_s}(E) = \int_0^\infty d\chi W_{\nu_s}([1+z]E, z), \quad (2.2)$$

where the window function $W_{\nu_s}(E, z)$ is

$$W_{\nu_s}(E, z) = \frac{\Omega_{\text{dm}} \rho_c \Gamma_{\nu_s}}{2(2\pi)^{3/2} m_{\nu_s} (1+z) \sigma_E} \exp \left[-\frac{(E - m_{\nu_s}/2)^2}{2(1+z)^2 \sigma_E^2} \right]. \quad (2.3)$$

¹ The lower limit for the redshift integration in Eqs. (2.1) is chosen to be $z = 0.003$. The mean intensity, as well as the angular power spectrum at high multipoles, are shown to be insensitive to this choice (e.g., [47]). See also the window function dependence on z in the right panel of Fig. 3.

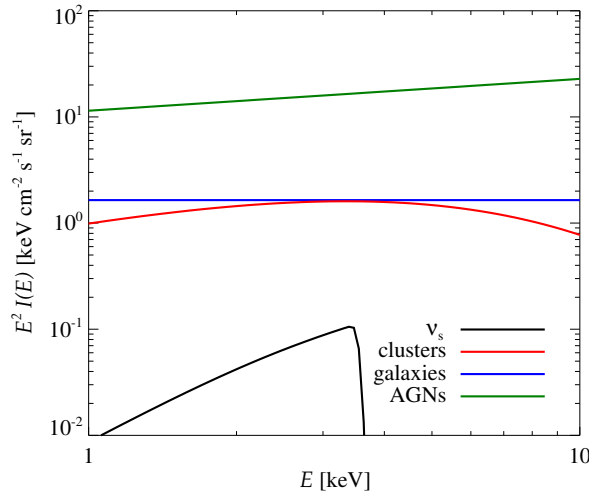


Figure 1. Contributions to the CXB mean intensity as a function of energy. We show the sterile neutrino signal for our reference scenario as described in the text (motivated by the findings of Refs. [15, 16]), compared with other astrophysical contributions: unresolved AGNs and galaxies, and galaxy clusters (both resolved and unresolved).

We adopt $\sigma_E = 0.138 \text{ keV}/\sqrt{8 \ln 2} = 0.0586 \text{ keV}$ corresponding to the energy resolution expected for *eROSITA* [45] at 6 keV.² As expected, Eqs. (2.2) and (2.3) show that, for a given energy E , the dominant contribution come mainly from redshifts around $z = m_{\nu_s}/2E - 1$.

Fig. 1 shows the mean intensity due to sterile neutrino decays, for a mass 7.12 keV and $\sin^2 2\theta = 7.6 \times 10^{-11}$, which will be our *reference scenario* motivated by the findings in Refs. [15, 16], compared with the CXB contribution from AGNs, galaxies, and galaxy clusters (these background components will be discussed in sections 2.2–2.4). The sterile neutrino component is completely subdominant, being smaller by two orders of magnitude with respect to the dominant AGN contribution, even at the peak energy around 3.5 keV.

2.2 Active galactic nuclei

AGNs are believed to provide the dominant contribution to the measured CXB [48–50]. We are here interested in the contribute from *unresolved* AGNs, since we can assume that all resolved point sources can be masked before performing the angular power-spectrum analysis. The unresolved contribution is extrapolated from the resolved one. Deep X-ray surveys suggest that the unresolved component contributes 76% to 82% in the 0.5–2 keV and 2–8 keV energy bands to the overall CXB, respectively [51].

We describe AGNs via their X-ray luminosity function (XLF) defined as the co-moving number density per unit logarithmic luminosity range $\Phi_{\text{AGN}}(L_X, z) \equiv dn_{\text{AGN}}/d \log_{10} L_X$. There are several parameterisations for the XLF and we adopt the Luminosity And Density

² Value taken from <http://www.mpe.mpg.de/455799/instrument>. We approximate the energy resolution as being constant in our energy range of interest, while in reality it improves at lower energies and worsen at higher energies. For example, in the case of *XMM-Newton* (see the *XMM-Newton* Users’ Handbook), the FWHM energy resolution at 1, 6 and 10 keV is about 70, 150 and 180 eV, respectively.

Evolution (LADE) model [52]:

$$\Phi_{\text{AGN}}(L_X, z) = K(z) \left[\left(\frac{L_X}{L_\star(z)} \right)^{\gamma_1} + \left(\frac{L_X}{L_\star(z)} \right)^{\gamma_2} \right]^{-1}, \quad (2.4)$$

where $K(z) = 10^{-4.53-0.19(1+z)} \text{ Mpc}^{-3}$, $\gamma_1 = 0.62$, and $\gamma_2 = 3.01$. The characteristic luminosity $L_\star(z)$, where the power-law break happens, depends on redshift and is parameterised as

$$L_\star(z) = L_0 \left[\left(\frac{1+z_c}{1+z} \right)^{p_1} + \left(\frac{1+z_c}{1+z} \right)^{p_2} \right]^{-1}, \quad (2.5)$$

where $L_0 = 10^{44.77} \text{ erg s}^{-1}$, $z_c = 0.75$, $p_1 = 6.36$, and $p_2 = -0.24$. Note that this XLF refers to luminosities integrated between $E_{\text{min}} = 2 \text{ keV}$ and $E_{\text{max}} = 10 \text{ keV}$ in the AGN rest frame.

The purpose of the current study is not to get a precise estimate of the mean intensity of unresolved AGNs, but to show the power of angular fluctuation to identify sterile neutrino dark matter. Therefore, we simply assume that each AGN features a simple power-law spectrum, $E^{-\Gamma}$, with a spectral index $\Gamma = 1.7$ in the relevant X-ray energy range (e.g., [53]). With this assumption, the differential luminosity at an energy E (defined as a number of photon emitted per unit time and per unit energy range), at redshift z , is

$$\mathcal{L}_X(E, z) = L_X \frac{2 - \Gamma}{E_{\text{max}}^{2-\Gamma} - E_{\text{min}}^{2-\Gamma}} E^{-\Gamma}, \quad (2.6)$$

where L_X denotes the luminosity used in Eq. (2.4). The mean AGN intensity is then calculated, similarly to Eq. (2.2), as³

$$I_{\text{AGN}}(E) = \int_0^\infty d\chi W_{\text{AGN}}([1+z]E, z), \quad (2.7)$$

where the AGN window function is given as

$$W_{\text{AGN}}(E, z) = \frac{1}{4\pi \ln 10} \int_{L_{X,\text{min}}}^{L_{X,\text{max}}} \frac{dL_X}{L_X} \Phi_{\text{AGN}}(L_X, z) \mathcal{L}_X(E, z). \quad (2.8)$$

For the lower and upper limit of luminosity integration, we adopt $L_{X,\text{min}} = 10^{41} \text{ erg s}^{-1}$ and

$$L_{X,\text{max}}(z) = \frac{4\pi d_L^2 F_{\text{sens}}}{(1+z)^{2-\Gamma}} \frac{E_{\text{max}}^{2-\Gamma} - E_{\text{min}}^{2-\Gamma}}{\tilde{E}_{\text{max}}^{2-\Gamma} - \tilde{E}_{\text{min}}^{2-\Gamma}}, \quad (2.9)$$

respectively (e.g., [52]). F_{sens} is the flux sensitivity of the considered X-ray telescope, and we adopt $4.4 \times 10^{-14} \text{ erg cm}^{-2} \text{ s}^{-1}$ for the energy range between $\tilde{E}_{\text{min}} = 0.5 \text{ keV}$ and $\tilde{E}_{\text{max}} = 2 \text{ keV}$ for eROSITA [45], which corresponds to the point-like sensitivity expected after the first six months of survey.⁴ The mean intensity of unresolved AGNs computed in this way is shown in Fig. 1. It is by far the dominant contribution to the CXB.

The AGN luminosity density of the adopted model has a 1σ uncertainty below 50% at low, $z \lesssim 0.2$, and high, $z \gtrsim 3$ redshifts, and below 20% in the middle range [52]. Therefore, while, as explained above, we refrain from a precise estimation of the unresolved AGN contribution, we note that our conclusions are robust against the present uncertainty.

³The lower limit for the redshift integration in Eq. (2.7) for AGNs, as well as for galaxies in section 2.3, is chosen to be 10^{-4} . This does not impact the calculations at all because all the AGNs and galaxies within this redshift give fluxes above the eROSITA sensitivity and hence they are completely resolved. See also the window function dependence on z in the right panel of Fig. 3.

⁴This implies that we will obtain slightly more conservative results than considering the sensitivity for the full four year survey, but we tested that the change in our final constraints is not significant (mostly since the result is limited by other factors, see discussion below).

2.3 Galaxies

Galaxies are also X-ray sources as they host X-ray binaries. The flux distribution of galaxies approaches that of AGNs at the faint end [51]. We adopt the XLF (in the rest-frame energy range band 0.5–2 keV) from Ref. [54], where the redshift evolution was studied from a galaxy sample below $z \approx 1$. The galaxy XLF is well represented with the following log-normal distribution function:

$$\Phi_{\text{gal}}(L_X, z) = \Phi_{\star} \left(\frac{L_X}{L_{\star}(z)} \right)^{1-\alpha} \exp \left[-\frac{1}{2\sigma^2} \ln^2 \left(1 + \frac{L_X}{L_{\star}(z)} \right) \right], \quad (2.10)$$

where $\Phi_{\star} = 10^{-2.23} \text{ Mpc}^{-3}$, $\alpha = 1.43$, and $\sigma = 0.72$. The characteristic luminosity L_{\star} evolves with redshifts while Φ_{\star} is constant (pure-luminosity evolution), and its evolution is parameterised as $L_{\star} = 10^{39.74} \text{ erg s}^{-1} [(1+z)/1.25]^{1.9}$.

The CXB mean intensity $I_{\text{gal}}(E)$, as well as its window function $W_{\text{gal}}(E, z)$, are computed in the same way as for the case of AGNs, by using the galaxy XLF $\Phi_{\text{gal}}(L_X, z)$ in Eqs. (2.7) and (2.8). This time, however, we adopt a E^{-2} spectrum [55], and thus the differential luminosity is given by

$$\mathcal{L}_X(E, z) = L_X \frac{E^{-2}}{\ln(E_{\text{max}}/E_{\text{min}})}, \quad (2.11)$$

where $E_{\text{min}} = 0.5 \text{ keV}$ and $E_{\text{max}} = 2 \text{ keV}$, and the upper limit of the luminosity integration is simply computed as $L_{X,\text{max}}(z) = 4\pi d_L^2 F_{\text{sens}}$, with $F_{\text{sens}} = 4.4 \times 10^{-14} \text{ erg cm}^{-2} \text{ s}^{-1}$ as for AGNs. The mean intensity of unresolved galaxies computed in this way is shown in Fig. 1. It is only about 10% of the emission from unresolved AGNs, but still an order of magnitude above our reference sterile neutrino signal. Also in this case, the 1σ uncertainty on the luminosity density is below 50% [54] and, therefore, our conclusions are robust.

2.4 Clusters of galaxies

Galaxy clusters are prominent X-ray emitters as the ambient gas, the intra-cluster medium (ICM), is a hot thermal plasma radiating bremsstrahlung emission (see [56] for a review). Indeed, X-ray observations are one of the main method to identify clusters. Clusters also represent some of the most promising targets to identify sterile neutrino dark matter, or any decaying dark matter candidate, as this process is directly proportional to the halo mass and they indeed are the most massive halos in the Universe.

Future X-ray instruments will help in narrowing down the contribute of galaxy clusters to the CXB. In fact, *eROSITA* is predicted to be able to resolve *all* galaxy clusters in the Universe [45]. However, differently from the previous cases of AGNs and galaxies, we must here consider the whole population of resolved *and* unresolved clusters and their thermal X-ray emission. This is because one of the questions here is: do clusters of galaxies also represent the bulk of the angular power spectrum for the sterile neutrino dark matter, and, therefore, is their thermal bremsstrahlung emission to be considered a dominant background in this approach? We underline that the bremsstrahlung emission depends on the gas density squared, which implies that significant morphological differences between a dark matter decay signal and the gas emission are expected.

Following the above notation, the mean cluster X-ray intensity due to bremsstrahlung radiation is given by⁵

$$I_{\text{cl}}(E) = \int_0^\infty d\chi W_{\text{cl}}([1+z]E, z) \langle \rho_{\text{gas}}^2 \rangle, \quad (2.12)$$

where ρ_{gas} is the ICM density, and

$$\langle \rho_{\text{gas}}^2 \rangle = \left(\frac{1}{\Omega_b \rho_c} \right)^2 \int dM_{200} \frac{dn}{dM_{200}} \int dV \rho_{\text{gas}}^2(r|M_{200}), \quad (2.13)$$

with integration boundaries that are discussed below. The cluster bremsstrahlung window function is

$$W_{\text{cl}}(E, z) = \frac{(\Omega_b \rho_c)^2}{4\pi} k_{\text{ff}} \frac{(k_B T_{\text{gas}})^{-1/2}}{E} \exp\left(-\frac{E}{k_B T_{\text{gas}}}\right), \quad (2.14)$$

where $k_B T_{\text{gas}}$ is the ICM temperature in keV. We define $k_{\text{ff}} = 9.5 \times 10^{32} g_{\text{ff}}$ (adapted from [58]), where $g_{\text{ff}} = 1.1$ is the Gaunt factor for the free-free emission, such that $I_{\text{cl}}(E)$ is expressed in $\text{cm}^{-2} \text{s}^{-1} \text{sr}^{-1} \text{keV}^{-1}$.

Our expression for the bremsstrahlung emission do not consider atomic line transitions in the ICM. This simplification is needed in order to treat the problem analytically. Atomic line transitions depend on temperature and mass of the cluster, and on the density squared as bremsstrahlung. The exclusion of atomic lines will hence have no impact on our study of morphological differences in the angular power spectrum for the different components. One might worry that our side-band analysis of section 5, which takes into account spectral information, is significantly affected by this approximation. However, as we will see, even neglecting entirely galaxy clusters in the analysis does not change much the final results. Hence, we believe that avoiding the transition lines does not impact much on this first study that we attempt here.

The adopted halo mass function dn/dM_{200} in Eq. (2.13), which will be later also used for the sterile neutrino angular power spectrum calculation, is based on the Tinker formalism [59] and obtained through the online application from [60]. In Eq. (2.13), the mass function is integrated above $M_{200}^{\text{cl,min}} \times h = 10^{14} M_\odot$, while the volume integral is within R_{200} . The transition between galaxy groups and galaxy clusters is not sharp or well-defined, and with the chosen $M_{200}^{\text{cl,min}}$ we already include large galaxy groups in the integration.

Finally, we need a prescription for the ICM density and temperature. We adopt the phenomenological model of [61], which is based on X-rays observations, and allows to assign a gas density (and temperature) to any galaxy cluster using its mass only, in such a way that the observed X-ray and Sunyaev-Zel'dovich scaling relations are correctly reproduced within about 20%. Following [61], we also statistically divide the cluster population in half merging clusters and half relaxed clusters, which are characterised by centrally cored and centrally peaked gas densities, respectively. This prescription needs however the clusters' mass as M_{500} which we obtain from M_{200} using the method in [62]. As a result, we find that the mean intensity of galaxy clusters, as shown in Fig. 1, is at the level of unresolved galaxies.

⁵The lower limit for the redshift integration in Eq. (2.12) is chosen to be $z = 0.01$ as the closest known galaxy clusters (see, e.g., [57]).

3 Auto-correlations of the angular power spectrum

Discussing the auto-correlation angular power spectrum of the different signal and background contributions to the CXB is useful for identifying the components that will yield the strongest contrast at a given angular scale $\theta = \pi/\ell$, where ℓ is the multipole. As usual, we define the intensity angular power spectrum of the signal and background fluxes as

$$C_\ell \equiv \langle |a_{\ell m}|^2 \rangle, \quad (3.1)$$

where the $a_{\ell m}$ are given by the decomposition of the flux into spherical harmonics $Y_{\ell m}$, namely

$$a_{\ell m} = \int d\Omega_{\mathbf{n}} I(\mathbf{n}) Y_{\ell m}^*(\mathbf{n}). \quad (3.2)$$

The auto-correlation angular power spectrum of a given source population A ($= \nu_s$, AGN, gal, cl) is then computed as [34, 63]

$$C_\ell^A(E) = \int_0^\infty \frac{d\chi}{\chi^2} W_A([1+z]E, z)^2 P_A\left(k = \frac{\ell}{\chi}, z\right), \quad (3.3)$$

where $P_A(k, z)$ is the power spectrum of the source A at wave number k and redshift z . In the halo model, the latter can be divided into one- and two-halo terms, $P_A = P_A^{1h} + P_A^{2h}$ (higher halo terms are negligible). In the case of dark matter decay, it is the nonlinear matter power spectrum ($P_{\nu_s} = P_\delta$) modelled as [64]

$$\begin{aligned} P_\delta^{1h} &= \left(\frac{1}{\Omega_{\text{dm}} \rho_c} \right)^2 \int dM_{200} \frac{dn}{dM_{200}} \left[\int 4\pi r^2 dr \rho_{\text{dm}}(r) \frac{\sin(kr)}{kr} \right]^2, \\ P_\delta^{2h} &= \left[\left(\frac{1}{\Omega_{\text{dm}} \rho_c} \right) \int dM_{200} \frac{dn}{dM_{200}} b(M_{200}, z) \int 4\pi r^2 dr \rho_{\text{dm}}(r) \frac{\sin(kr)}{kr} \right]^2 P_{\text{lin}}(k, \chi), \end{aligned} \quad (3.4)$$

where the mass integration starts from $M_{200}^{\nu_s, \text{lim}} \times h = 10^6 \text{ M}_\odot$, the radial integration goes up to R_{200} , $P_{\text{lin}}(k, \chi)$ is the linear matter power spectrum (obtained from [60]), and $b(M_{200}, z)$ is the linear bias [65]. The lower mass limit for the integration of the sterile neutrinos, which represent effectively a WDM candidate, can be chosen to be around 10^6 – 10^8 M_\odot (e.g., [66, 67]). Since the precise choice of the lower mass limit does not affect the auto- and cross-power spectra that we will discuss, we adopt for definiteness $M_{200}^{\nu_s, \text{lim}} \times h = 10^6 \text{ M}_\odot$. Note also that our $P_{\text{lin}}(k, \chi)$ is obtained for a CDM scenario, but as the WDM halo mass function starts to drop below its CDM counterpart around 10^9 M_\odot [67], this choice of P_{lin} has no impact on our conclusions. The negligible relevance of the two above choices, $M_{200}^{\nu_s, \text{lim}}$ and $P_{\text{lin}}(k, \chi)$, is made clear by Fig. 7 which shows that the dominant contribution to the sterile neutrino power spectrum comes from halos with $M_{200} \times h \gtrsim 10^{11} \text{ M}_\odot$.

In order to calculate the angular power spectrum of Eqs. (3.5), we need the distribution of dark matter in halos ρ_{dm} . For the present study, we will adopt the Navarro-Frenk-White (NFW) profile [68], which is given by

$$\rho_{\text{dm}}(r) = \frac{\rho_s}{(r/r_s)(r/r_s + 1)^2}, \quad (3.5)$$

where ρ_s and r_s denote the scale density and radius, respectively. We use throughout the parameters M_{200} and R_{200} to indicate the halo mass and radius, respectively. Hence, our

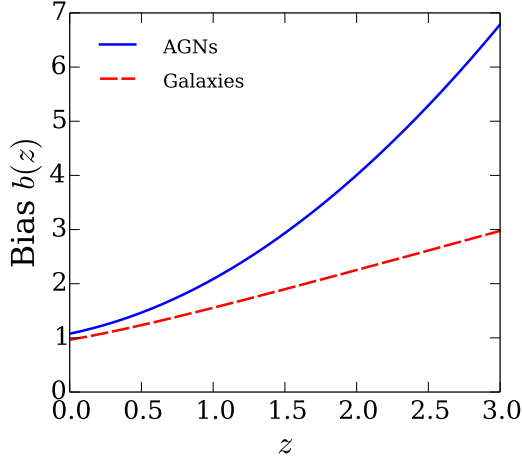


Figure 2. Bias of the X-ray AGNs and galaxies as a function of redshift z .

scale radius is defined as $r_s = R_{200}/c_{200}$, where $c_{200}(M_{200}, z)$ is the concentration parameter [69]. With this, one can show that, for a given halo mass M_{200} , the scale density is given by

$$\rho_s = \frac{M_{200}}{4\pi r_s^3} \left[\ln(1 + c_{200}) - \frac{c_{200}}{1 + c_{200}} \right]^{-1}. \quad (3.6)$$

In the case of clusters of galaxies, $P_{\text{Cl}}(k, \chi)$ is similar to that of Eqs. (3.5), but with $M_{200}^{\text{cl,lim}} \times h = 10^{14} M_{\odot}$. Additionally, $\rho_{\text{dm}}(r)$ has to be substituted by $\rho_{\text{gas}}(r)^2$ and $(1/\Omega_{\text{dm}}\rho_c)$ by $(1/\Omega_{\text{b}}\rho_c)^2$, and we assume that $P_{\text{lin}}(k, \chi)$ is related to the cluster power spectrum via the linear bias.

We assume that AGNs and galaxies are good tracers of the dark matter density, and thus $P_{\text{AGN,gal}}(k, z) = b_{\text{AGN,gal}}^2(z) P_{\delta}(k, z)$, where we again use Eq. (3.5) for the nonlinear power spectrum of dark matter density fluctuation δ . For the AGNs, we adopted the halo linear bias from [65] and assume that the X-ray AGNs reside in dark matter halos with mass of $10^{13.1} M_{\odot}$ [70]. For the X-ray emitting galaxies, we adopt the prescription given in [71]. The bias models for both AGNs and galaxies are shown in Fig. 2 as a function of redshift. The uncertainty on the AGN bias can be estimated to be below about 10%, while for the halo mass in which X-ray AGNs are supposed to reside it is of about 30% [70]. The model for the bias of the X-ray galaxies of Ref. [71] well reproduces measurements of star-forming and high- z Ly-break galaxies which in turn have uncertainties below about 20%. Note that the galaxy bias is very close to 1 for $z \lesssim 1$, which is the redshift range most interesting for dark matter searches.

Finally, since AGNs and galaxies are point-like sources, there is an additional shot-noise contribution to the angular power spectrum, which is independent of angular scale ℓ . This *Poisson* term is computed by (e.g., [63])

$$C_{\text{P}}^{\text{AGN,gal}}(E) = \frac{1}{(4\pi)^2 \ln 10} \int_0^{\infty} \frac{d\chi}{\chi^2} \int_{L_{\text{X,min}}}^{L_{\text{X,max}}} \frac{dL_{\text{X}}}{L_{\text{X}}} \Phi_{\text{AGN,gal}}(L_{\text{X}}, z) \mathcal{L}_{\text{X}}(E, z)^2. \quad (3.7)$$

So far, we discussed only the *differential* (in energy) angular power spectrum, but the same argument applies to the angular power spectrum *integrated* over a certain energy range.

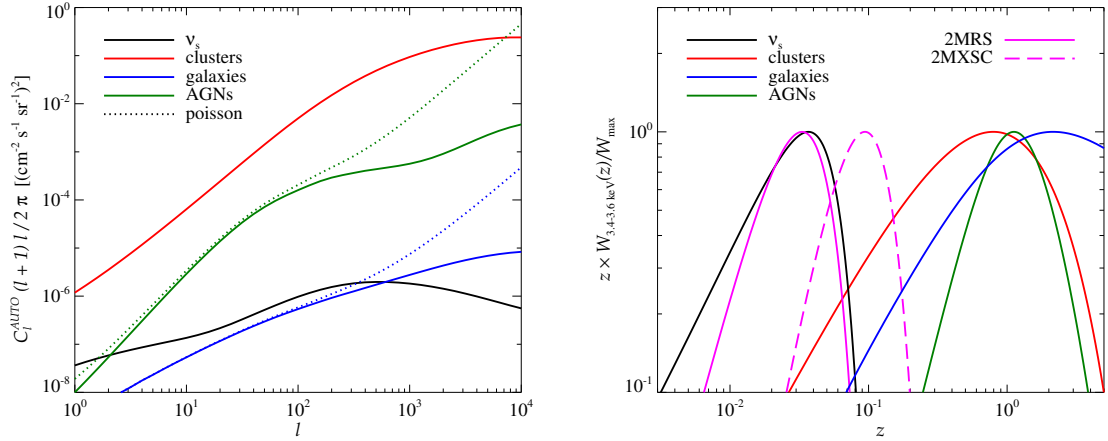


Figure 3. Left. Auto-correlation angular power spectrum of CXB due to sterile neutrino decays for our reference model, (unresolved) AGNs, (unresolved) galaxies, and (resolved and unresolved) clusters of galaxies in the 3.4 – 3.6 keV energy band. For AGNs and galaxies, both the correlation term (solid) and total including Poisson term (dotted) are shown. **Right.** Redshift-weighted window functions integrated in the 3.4 – 3.6 keV energy band and normalised at their maximum for sterile neutrino decays with our reference model, AGNs, galaxies, clusters of galaxies (fixing the ICM temperature to 5 keV), and 2MRS and 2MXSC catalogues.

One first integrates the window function W_A over the relevant energies, and then computes the power spectrum using Eq. (3.3). Similarly, for the Poisson term, one integrates \mathcal{L}_X over the chosen energy range and then computes the shot noise with Eq. (3.7). In order to emphasise the difference, we will in the following explicitly show the energy dependence, $C_\ell(E)$, when refereeing to differential power spectra, while the energy dependence is suppressed, C_ℓ , for the integrated quantities.

In the left panel of Fig. 3, we show the auto-correlation angular power spectrum integrated over the 3.4–3.6 keV energy band, adopting our reference model for the sterile neutrino decay. The component coming from sterile neutrinos is completely subdominant with respect to contributions from clusters at all multipoles, as well as from AGNs, and, to a lesser extent, from galaxies, for most angular ranges. Furthermore, we also show that at larger multipoles the contributions from the Poisson term become increasingly important and start to dominate. In the right panel of Fig. 3, we show the shape of the window function integrated in the 3.4–3.6 keV energy band for the different components, and for the 2MRS and 2MXSC galaxy catalogues that will be introduced in the next section.

Actually, the power spectrum of the sterile neutrino component can be obtained by using a non-linear matter power spectrum directly calculated with, e.g., the Code for Anisotropies in the Microwave Background (CAMB; <http://camb.info/>). We adopted the halo model approach in order to have control on the spatial part of the angular power spectrum calculation for clusters of galaxies, and kept this approach in all cases for consistency. In Fig. 4, we compare the sterile neutrino auto-correlation angular power spectrum obtained with the halo model approach to that obtained with the non-linear matter power spectrum from CAMB and find reasonably good agreement, to within a factor of less than two.

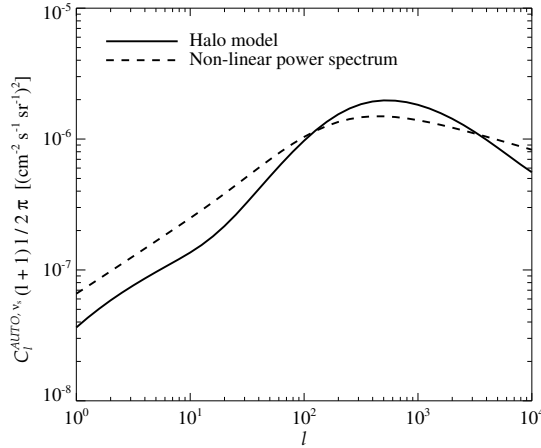


Figure 4. The auto-correlation angular power spectrum of sterile neutrino decays computed with the halo model (used in our main analysis) and with the non-linear matter power spectrum from CAMB, respectively.

4 Cross correlations with the 2MASS galaxy catalogues

We will now show that, since the signal from sterile neutrino decays follows the distribution of dark matter in the Universe, a cross-correlation between the X-ray signal and tracers of the dark matter distribution is a very promising strategy to isolate the dark matter contribution. To this end, we will compute the cross-correlation with large galaxy catalogues from the 2MASS survey [46], which in fact trace the dark matter distribution in the *local* Universe.

The 2MASS catalogue provides nearly complete information on the galaxy distribution for the local Universe. The 2MASS Redshift Survey (2MRS) [46] is based on spectroscopic redshift determination of $N_{2MRS} \approx 43500$ galaxies up to $z \approx 0.1$ with a sky coverage of 91%. The 2MRS galaxies follow approximately the redshift distribution given by

$$\frac{dN_{2MRS}}{dz} \propto z \exp \left(- \left[\frac{z}{z_{2MRS}} \right]^2 \right), \quad (4.1)$$

where $z_{2MRS} = 0.033$. For comparison, we also adopt the 2MASS Extended Source Catalogue (2MXSC), an even larger sample that contains $N_{2MXSC} \approx 770000$ galaxies with a sky coverage of 67% [72, 73], but with less accurate redshift determination through photometry. The redshift distribution of 2MXSC is approximately given by [73]

$$\frac{dN_{2MXSC}}{dz} \propto z^{1.9} \exp \left(- \left[\frac{z}{z_{2MXSC}} \right]^{1.75} \right), \quad (4.2)$$

where $z_{2MXSC} = 0.07$. We fix the normalisation of both the 2MRS and 2MXSC catalogues such that the redshift integration gives the total number galaxies N_{2MRS} and N_{2MXSC} , respectively.

The angular cross-power spectrum of a given source population A ($= \nu_s$, AGN, gal, cl) with the 2MRS or 2MXSC galaxies, labelled B, is therefore computed as [63]

$$C_\ell^{A,B}(E) = \int \frac{d\chi}{\chi^2} W_A([1+z]E, z) W_B(\chi) P_{A,B} \left(k = \frac{\ell}{\chi}, \chi \right), \quad (4.3)$$

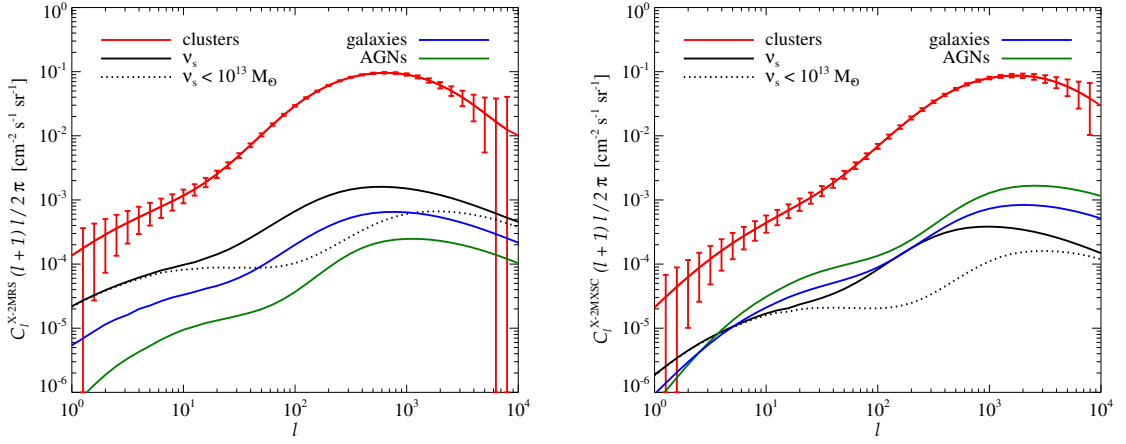


Figure 5. Cross-correlation angular power spectrum of CXB due to sterile neutrino decays for the reference model, (unresolved) AGNs, (unresolved) galaxies, and (resolved and unresolved) clusters of galaxies in the 3.4–3.6 keV energy band. For sterile neutrinos, we also show the case when the integration upper mass limit is fixed to $M_{200}^{\nu, \text{lim}} \times h = 10^{13} M_{\odot}$ (see main text for details). We overlay to the cluster component the error bars $\Delta C_{\ell}/\sqrt{\Delta \ell}$, with $\Delta \ell = \ell/2$ the bin size, estimated from the diagonal part of the covariance matrix for the total power of Eq. 5.1. **Left:** Cross correlation with 2MRS. **Right:** Cross correlation with 2MXSC.

where $W_B(\chi) = (dz/d\chi)(dN_B/N_B dz)$ is the galaxy catalogue window function (normalised to unity), and $P_{A,B}(k, z)$ is the cross-power spectrum. For the cross-power spectrum, we adopt for the galaxy catalogues bias $b_{2\text{MRS}/2\text{MXSC}} = b_{\text{gal}}$. In case of cross-correlation with clusters of galaxies, the cross-power spectrum, $P_{\text{cl},B} = P_{\text{cl},B}^{\text{1h}} + P_{\text{cl},B}^{\text{2h}}$, reads

$$P_{\text{cl},B}^{\text{1h}} = \left(\frac{1}{\Omega_b \rho_c} \right)^2 \frac{b_{\text{gal}}(z)}{\Omega_{\text{dm}} \rho_c} \int dM_{200} \frac{dn}{dM_{200}} \times \left[\int 4\pi r^2 dr \rho_{\text{gas}}^2(r) \frac{\sin(kr)}{kr} \right] \left[\int 4\pi r^2 dr \rho_{\text{dm}}(r) \frac{\sin(kr)}{kr} \right], \quad (4.4)$$

$$P_{\text{cl},B}^{\text{2h}} = \left[\left(\frac{1}{\Omega_b \rho_c} \right)^2 \int dM_{200} \frac{dn}{dM_{200}} b(M_{200}, z) \int 4\pi r^2 dr \rho_{\text{gas}}^2(r) \frac{\sin(kr)}{kr} \right] \times \left[\frac{b_{\text{gal}}(z)}{\Omega_{\text{dm}} \rho_c} \int dM_{200} \frac{dn}{dM_{200}} b(M_{200}, z) \int 4\pi r^2 dr \rho_{\text{dm}}(r) \frac{\sin(kr)}{kr} \right] P_{\text{lin}}(k, \chi). \quad (4.5)$$

In the case of cross correlation with sterile neutrino dark matter, the cross-power spectrum reads as in Eqs. (4.4) and (4.5), but one has to substitute $\rho_{\text{gas}}^2(r)$ with $\rho_{\text{dm}}(r)$ and $(1/\Omega_b \rho_c)^2$ with $(1/\Omega_{\text{dm}} \rho_c)$. For the cross-correlation with X-ray AGNs or galaxies, we have $P_{\text{AGN/gal},B}(k, z) = b_{\text{AGN/gal}}(z) b_{2\text{MRS}/2\text{MXSC}}(z) P_{\delta}(k, z)$.

We show in Fig. 5 the cross-correlation angular power spectrum, $C_{\ell}^{A,B}$, cross-correlated with 2MRS (left panel) and 2MXSC (right panel) galaxies, integrated over 3.4–3.6 keV, and compare the sterile neutrino component with AGNs, galaxies and clusters. The shapes of the power spectra are similar for all components, as they trace the dark matter distribution quite well, while some deviations are observed for clusters where the emission depends on the gas density squared.

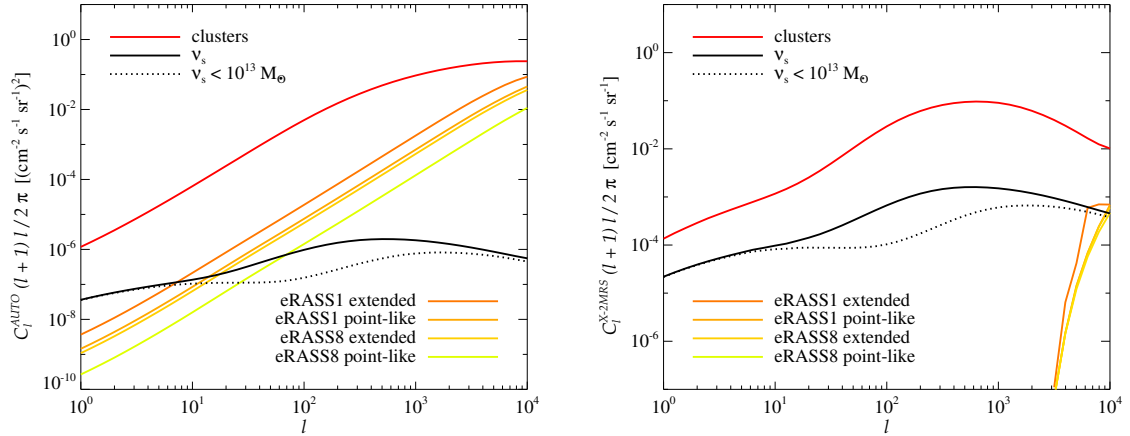


Figure 6. Left: Auto-correlation power spectrum of sterile neutrino decays, for the reference model, and clusters of galaxies in the 3.4–3.6 keV energy band. For clusters of galaxies, we show the case when all resolved and unresolved objects are included, and the cases where we exclude the objects exceeding the *eROSITA* expected sensitivities (for point-like/extended sources and eRASS1/eRASS8 results). For sterile neutrinos, we also show the case when the integration upper mass limit is fixed to $M_{200}^{\nu, \text{lim}} \times h = 10^{13} M_\odot$. **Right:** The same but for cross-correlation with 2MRS.

We find that the cross-correlation signal of (resolved and unresolved) galaxy clusters dominates over all components at all multipole scales. At the same time, the sterile neutrino component, subdominant in the auto-correlation, is now comparable to the AGN and galaxy components. In particular, the sterile neutrino component dominates over the AGNs and galaxies over all multipoles for the cross correlation with 2MRS. When cross-correlating with 2MXSC, AGNs and galaxies dominate over the sterile neutrino component at all multipoles above $l \approx 5$, while being still comparable. This can be explained by the fact that unresolved AGNs and galaxies grow in number with redshift, therefore correlating more with the higher redshift sample of 2MXSC. At the same time, most of the power from sterile neutrinos comes from low redshifts, which causes the 2MXSC cross-correlation power spectrum to be lower with respect to the 2MRS case. This can be seen also looking at the redshift variations of the window functions of different components in the right panel of Fig. 3.

We also try an additional approach to further reduce the contribution from clusters. This is simply to exclude completely clusters of galaxies from such an analysis. One would think that by doing so, we would exclude most of the sterile neutrino signal too, but we will see that the contrary is true. In Fig. 6, we show how the contribution from clusters of galaxies can be dramatically lowered when excluding clusters that will be resolved by *eROSITA*. We consider both point-source and extended expected sensitivities [45] to bracket the case of extended and smaller, far-away point-like clusters, from the first six months of survey (eRASS1) and the complete survey (eRASS8). The left panel of Fig. 6 shows the auto-correlation power spectra, while the right panel shows the cross-correlation with 2MRS. We compare these with the sterile neutrino component, and with the same sterile neutrino component but integrated only up to $M_{200}^{\nu, \text{lim}} \times h = 10^{13} M_\odot$, effectively excluding all clusters of galaxies. The figures clearly show that excluding clusters of galaxies from such an analysis does not have a big impact on the magnitude of the sterile neutrino component, and, at the same time, that with the *eROSITA* survey it will be realistic to exclude them as all will be resolved. The

relative importance of galaxy clusters becomes even clearer when looking at the individual contributions from different halo sizes in Fig. 7 where we show that a large contribution to the sterile neutrino power spectra comes from galaxy-size halos. For completeness, we show the sterile neutrino component integrated only up to $M_{200}^{\nu,\text{lim}} \times h = 10^{13} \text{ M}_{\odot}$ also in the cross-correlation spectra of the above Fig. 5.

To conclude this section, in Fig. 8, we show the 2MRS (left) and 2MXSC (right) cross correlation $C_{\ell}^{\times}(E)$ at $\ell = 50$ as a function of energy. The cluster component dominates at all energies. The sterile neutrino component dominates over those of AGNs and galaxies around its peak energy for 2MRS, while it is just below for 2MXSC. This is due not only to the fact that high-redshift AGNs and galaxies cross-correlate more with the higher redshifts of 2MXSC, as discussed for Fig. 5, but also to the fact that, in this case, the sterile neutrino decay line is broader due to these higher redshifts too. Looking back at the 2MXSC cross correlation in the right panel of Fig. 5, we can argue that a energy range broader than 3.4–3.6 keV, better including the sterile neutrino decay line peak, would increase its cross-correlation with 2MXSC, but would also increase that of the other components. Note that the choice of $\ell = 50$ for Fig. 8 is arbitrary and done only with illustrative purposes. However, the behaviour at different multipoles is understandable noting the relative differences among different components in the cross-correlations of Fig. 5. This is particularly true for the case of the cross-correlation with 2MRS where the curves for the different components are remarkably similar at all scales.

Our main finding is that, although the sterile neutrino auto-correlation component is completely dominated by clusters, AGNs and galaxies (see Fig. 3), by taking the cross correlation, we are able to highlight it over the AGNs and galaxies. The contribution from clusters of galaxies is very strong also in the cross-correlation case. However, by completely excluding clusters of galaxies from such an analysis, which is a realistic assumption as *eROSITA* is expected to resolve them all, and reducing the sterile neutrino component analysis only to structures up to $M_{200}^{\nu,\text{lim}} \times h = 10^{13} \text{ M}_{\odot}$, we do not lose a significant fraction of sterile neutrino decays. In the next section, we will show that a detailed analysis will be able to identify the sterile neutrino dark matter over the backgrounds in both cases.

5 Detectability and projected limits

In this section, we finally study the sensitivity for sterile neutrino signals using the cross-correlation angular power spectrum. To this end, we perform a χ^2 fit to mock data in different energy ranges, with free normalisation of the individual background components and of the signal. We take properly into account the covariance of the different components, which is usually neglected.

As already mentioned, we take the soon-to-be-launched *eROSITA* as reference X-ray satellite. Therefore, we adopt an angular resolution $\sigma_b = 15''$ and an (FWHM) energy resolution of 138 eV. The angular and energy resolution have a mild dependence on energy in the range of interest (see [45] and Footnote 2), which we neglect for this work. The effective area is of the order of 500 cm^2 and the field of view (FoV) around $55'$ diameter, with a strong dependence on energy, and we adopt here the energy-dependent values for the grasp as given in [45]. The total observation time is assumed to be four years.

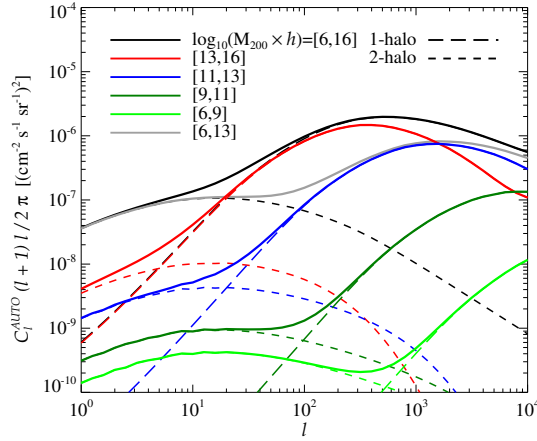


Figure 7. Contributions to the auto-correlation angular power spectrum for our reference sterile neutrino scenario split into different halo mass ranges. Note that for the mass range $10^6 - 10^{13} M_\odot$, only the total (1-halo + 2-halo) is shown. Note that our P_{lin} is obtained for a CDM scenario, therefore the contribution below $10^9 M_\odot$ is likely overestimated [67]. However, as clear from the figure, this regime has no impact on our conclusions regarding the auto- and cross-correlation power spectra.

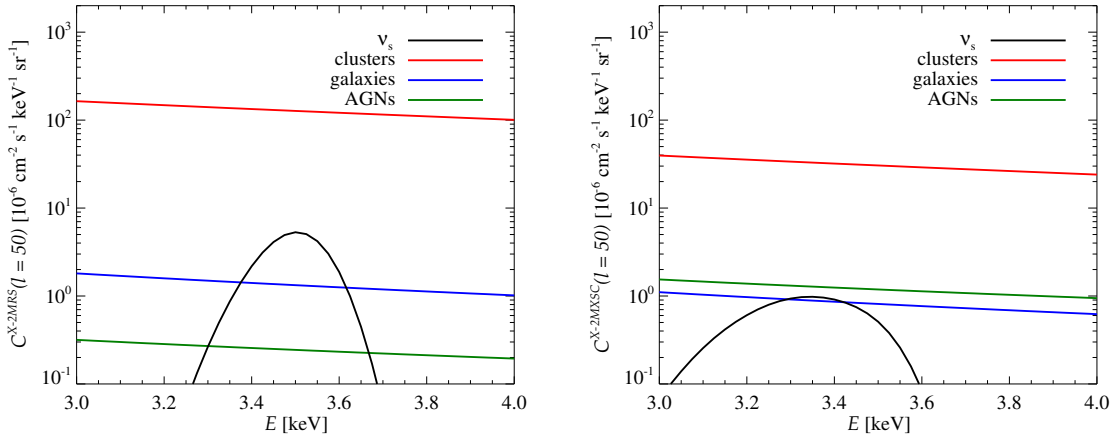


Figure 8. Angular cross-power spectrum for 2MRS (left) and 2MXSC (right) at $\ell = 50$ as a function of energy.

5.1 Statistical method

The relevant uncertainties that we have to consider in our statistical analysis come from the shot noise of the measured X-ray photons, the finite number of measured galaxies, and the cosmic variance. The X-ray shot noise affects different X-ray energy ranges differently, whereas galaxy shot noise and cosmic variance affect all energy ranges in the same way.

We perform a sideband analysis fitting the data in three energy ranges simultaneously. In this case the cross-correlation angular power spectrum $C_\ell^{\gamma:g}$ becomes a vector with three entries, and its variance is described by a 3×3 covariance matrix. This matrix is given by

(see Appendix A for details)

$$(\Delta C_{\ell}^{\gamma,g})_{ij}^2 = \frac{1}{(2\ell+1)f_{\text{sky}}} \left[C_{\ell i}^{\gamma,g} C_{\ell j}^{\gamma,g} + \left(\frac{C_{N i}^{\gamma} \delta_{ij}}{W_{\ell}^2} + \sqrt{C_{\ell i}^{\gamma} C_{\ell j}^{\gamma}} \right) (C_N^g + C_{\ell}^g) \right], \quad (5.1)$$

where $C_N^{\gamma} = 4\pi \langle I \rangle^2 / N_{\gamma}$ and $C_N^g = 4\pi / N_g$ are respectively the photon and galaxy count shot noise terms, and $\langle I \rangle$ is the average intensity of the total flux, as shown in Fig. 1, in a given energy range. The indices i and j refer to different energy ranges, and δ_{ij} is the Kronecker delta. Furthermore, f_{sky} denotes the fraction of the sky that was observed, and $W_{\ell} = \exp(-\sigma_b^2 \ell^2 / 2)$ is the detector window function of a Gaussian point-spread function. Therefore, note that the contribution from the photon shot-noise is diagonal, since the noise is independent for the various energy ranges, and different in each because the mean intensity is different. On the other hand, the galaxy shot noise affects the cross-correlation with photons from different energy ranges in the same way.

We perform our analysis on three reference energies for the sterile neutrino mass: $m_s = 2.0, 7.2$ and 18.0 keV. For each of the sterile neutrino masses, we define three energy bands that are centred on the line, and are at slightly lower and higher energies. These energy ranges are in keV units (low, central, high) = $(0.5\text{--}0.8, 0.9\text{--}1.1, 1.2\text{--}1.5)$, $(3.0\text{--}3.3, 3.4\text{--}3.6, 3.7\text{--}4.0)$ and $(8.5\text{--}8.8, 8.9\text{--}9.1, 9.2\text{--}9.5)$. We show the auto- and 2MRS cross-correlation spectra for the $0.9\text{--}1.1$ and $8.9\text{--}9.1$ keV energy bands in Appendix B. The central band covers most of the signal as shown in the left panel of Fig. 8 for 2MRS. In the following, we will discuss results only for the 2MRS catalogue for simplicity as the results that one would obtain for the 2MXSC catalogue would be less constraining due to the different redshift distribution of the latter as explained and showed in the previous sections.

We treat the instrumental backgrounds in a simple way, by increasing the photon shot-noise term, $C_{N i}^{\gamma}$, appropriately. We adopt here the factors 5.0, 3.0 and 100 for 2.0, 7.2 and 18.0 keV sterile neutrinos, respectively. At these energies, the background is dominated by Galactic thermal emission, the CXB, and the particle background, respectively [45].

The χ^2 function that we use for the sensitivity estimates is given by

$$\chi^2 = \sum_{\ell=\ell_0}^{\ell_1} \sum_{i,j=1}^3 (\bar{C}_{\ell i}^{\gamma,g} - C_{\ell i}^{\gamma,g}(\theta)) [(\Delta C_{\ell}^{\gamma,g})^2]_{ij}^{-1} (\bar{C}_{\ell j}^{\gamma,g} - C_{\ell j}^{\gamma,g}(\theta)), \quad (5.2)$$

where the first term in the first factor denotes the measured cross-correlation spectrum, and the second term is the model. The sum is taken over the angular range $\ell = [\ell_0, \ell_1]$ and over all three energy bands. Our default angular range, to which we will refer as baseline case, is given by $\ell_0 = 10^2$ and $\ell_1 = 10^4$.

The model is a linear combinations of the contributions from sterile neutrinos, unresolved AGNs and galaxies, and (resolved and unresolved) cluster emission. Here, we are interested in deriving projected upper limits on a sterile neutrino component. We hence generate mock data (Asimov data) with the sterile neutrino flux set to zero, and adopt the standard $\Delta\chi^2$ method to derive 95% CL upper limits. To this end, we increase the signal flux while refitting the other parameters until the χ^2 function changes by $\Delta\chi^2 = 2.71$.

5.2 Projected limits

The resulting projected limits are shown in Fig. 9. Most interestingly, we find that for our baseline analysis *eROSITA* is sensitive to our reference sterile neutrino scenario, which is

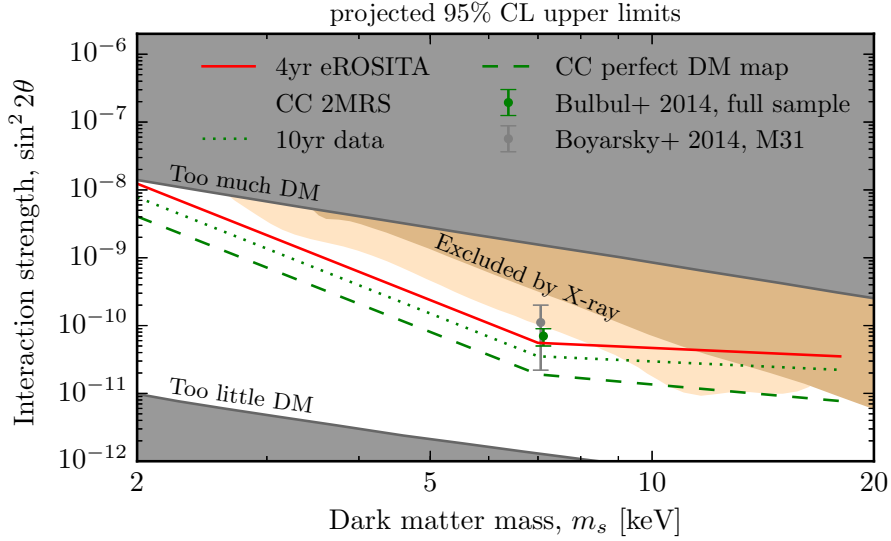


Figure 9. Projected 95% CL upper limits on the sterile neutrino mixing angle as function of the sterile neutrino mass. For the baseline results (red solid line) we assume 4 yr of data taking with *eROSITA*, and a sideband analysis of the cross-correlation (CC) angular power spectrum with the 2MRS catalogue as discussed in the text. This is just on top of the tentative 3.5-keV line reported by different groups. For comparison, we also show the limits obtained for 10 yr of data taking (green dotted line), and when cross-correlating 4 yr data with a hypothetical *perfect* model of the dark matter decay signal (dashed green line; no shot noise, same window function as for 2MRS and negligible bias). We derived projected limits for three reference energies and interpolate otherwise. For comparison, we also show regions that are excluded by over- or underproducing the observed DM relic density (grey areas), and regions excluded by previous X-ray observations (light brown regions), following Refs. [12, 13, 16].

motivated by the findings of Refs. [15, 16]. If the claimed 3.5 keV feature is indeed due to dark matter decay, *eROSITA* should be able to see it.

We discuss now briefly what are the limiting factors for the sensitivity of our baseline analysis, and how this could be further improved. In Fig. 9, we also show the limits that would be obtained if either the galaxy shot noise or the photon shot noise terms are set to zero. These correspond, respectively, to the cases of either perfect knowledge about the dark matter distribution (no shot noise, same window function as for 2MRS, and negligible bias; note that the latter is close to one for galaxies, see section 3), or 10 yr observation time. We find that the galaxy noise term is the most limiting factor for current searches, suggesting that improved measurements of the dark matter distribution in the local Universe would be of great help when performing cross-correlation searches with *eROSITA* data.

Finally, for comparison, we show in Fig. 10 the limits that can be obtained when masking out all massive clusters with masses above $M_{200} \times h = 10^{13} M_{\odot}$, for the cross-correlation with the hypothetical perfect DM tracer. The limits obtained in this way are only a factor $\lesssim 2$ less constraining than what we found with our baseline analysis (with the hypothetical perfect DM tracer). This suggests that a good sensitivity to dark matter signals can be obtained even if galaxy clusters, with potentially problematic background lines from atomic transitions,

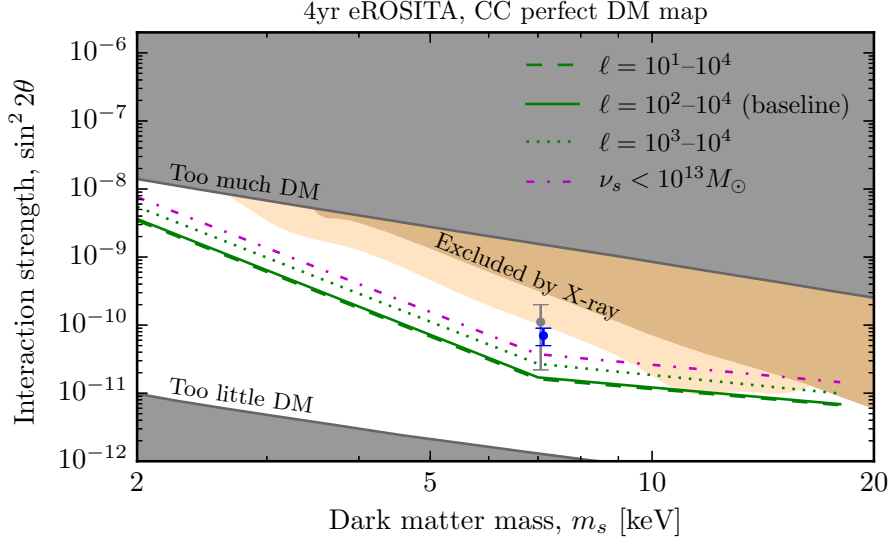


Figure 10. Same as Fig. 9, for 4 yr of eROSITA data and cross-correlation (CC) with a perfectly modelled dark matter signal. We show the impact of varying the considered angular range (green lines), finding that the impact of angular scales $\ell < 100$ is rather minor. We also show how the limits change when masking out *all* halos with masses above $M_{200} \times h = 10^{13} M_{\odot}$ (magenta dash-dotted line). The projected limits weaken then by a factor of two, but are then unaffected by the strong astrophysical line emission that is associated with the thermal emission from galaxy clusters.

are excluded from such an analysis as we also showed in Figs. 3, 5 and 7. Note, however, that in the current situation where our knowledge of the local dark matter distribution is limited, the exclusion of the most massive halos from this analysis is not advisable as can be argued looking at our baseline model in Fig. 9: a factor of 2 worsening could compromise the ability of testing the 3.5-keV line interpretation. We finally show that including larger angles (smaller ℓ) in the analysis would not improve the sensitivity further, whereas the ranges $\ell = 10^2-10^3$ and $\ell = 10^3-10^4$ are approximately equally important.

In general, we find that the cross-correlation analysis can significantly improve the present constraints on sterile neutrinos below about 10 keV, while above these energies the constraints that we obtain are comparable or worse than what can be obtained by pointed X-ray observations (e.g., from Refs. [12, 13, 16] as shown in Figs. 9 and 10) as our approach becomes dominated by the instrumental background (see also Fig. 12 in Appendix B).

6 Conclusions

Motivated by claims of an unidentified 3.56-keV X-ray line found in several galaxies and clusters of galaxies, and its interpretation in terms of the decay of sterile neutrino dark matter [15, 16], we investigated for the first time the possibility of searching for such signatures using upcoming full-sky observations of the cosmic X-ray background. We computed both the auto- and cross-correlation angular power spectra, where for the latter we adopted a nearby all-sky galaxy catalogue, for the sterile neutrino component and astrophysical backgrounds.

As astrophysical components that give contributions to the X-ray background, we considered AGNs, galaxies (powered by X-ray binaries), and thermal bremsstrahlung emission from clusters of galaxies. The combinations of these three sources, in particular AGNs, give the dominant contribution to the mean background intensity, and the component of the sterile neutrino decays, with inferred parameters from [15, 16], gives only $\sim 1\%$ contribution, even at the peak energy around 3.5 keV.

We found that the auto-correlation angular power spectrum is dominated by the galaxy cluster component at almost all angular scales, as they are a rare (more rare than AGNs and galaxies) and individually bright sources. AGNs dominate over galaxies and the sterile neutrino decays, and the latter gives only a small contribution to the total angular power, comparable to that of galaxies. Since *eROSITA* will resolve most galaxy clusters through their thermal emission, the cluster component could be in principle excluded from the analysis. Even in that case, however, a large contribution from the unresolved AGNs would hide the underlying dark matter component almost completely.

Since the window function of the spectroscopic 2MASS galaxy catalogue has considerable overlap with that of the sterile neutrino decays, taking the cross-correlation with the 2MASS galaxies efficiently highlight the dark matter component. In fact, we found that the cross-correlation power spectrum of sterile neutrino decays is larger than that of both AGNs and galaxies. The cluster component is still larger than the sterile neutrino one. However, when masking all the clusters that will be resolved with *eROSITA*, we found that the dark matter component (computed from all the halos up to $M_{200} \times h = 10^{13} M_{\odot}$) becomes the largest in the cross-correlation power spectrum at almost all angular scales.

Using the above results, we performed a χ^2 analysis in order to estimate the expected sensitivity of *eROSITA* for sterile neutrino searches. We perform a sideband analysis using three energy ranges — one centred on the potential line and other two, higher and lower, bands to calibrate continuous astrophysical components. We find that when cross-correlating *eROSITA* data with the 2MASS galaxies, the projected 95% CL upper limits after four years of observation are cutting into the parameter region of the recently claimed 3.56 keV sterile neutrino decay line [15, 16]. Moreover, we show that the cross-correlation analysis can significantly improve the present constraints on sterile neutrinos below about 10 keV, while above these energies our approach becomes dominated by the instrumental background and the corresponding constraints are not as competitive with respect to pointed X-ray observations. We also find that the masking of galaxy clusters does not improve the constraints, unless a better knowledge of the local dark matter distribution is achieved. In fact, the main limitation comes from the shot noise associated with the finite number of galaxies in the 2MASS catalogue. Indeed, we showed that when using shot-noise free tracers for dark matter, i.e., having a perfect knowledge of the local dark matter distribution with no bias, the projected limits improve significantly, allowing *eROSITA* to put stringent constraints on the possible sterile neutrino signal. *Hence, in order to ensure that the potential of eROSITA and other full-sky X-ray surveys is fully realised for dark matter searches, it is critical to obtain a detailed description of the dark matter distribution at low redshift, at galaxy and galaxy cluster scales, without the shot-noise limitations of the 2MASS catalogue.* To what extent this can be achieved by a combination of optical and X-ray observations (e.g., Ref. [32]), and of gravitational lensing [29, 33] will be discussed in a forthcoming publication [74].

Note added. In the final stages of our work we became aware of another group exploring a similar approach [75].

Acknowledgments

We would like to thank Andrea Chiappo, Marco Regis, Miguel-Angel Sanchez-Conde and Petr Tinyakov for useful discussions. FZ acknowledge the support of the Spanish MICINN Consolider-Ingenio 2010 Programme under grant MultiDark CSD2009-00064, AYA10-21231. This work was supported by the Netherlands Organization for Scientific Research (NWO) through one Veni (FZ) and two Vidi (SA and CW) grants.

A Treatment of correlated statistical uncertainties

We discuss briefly how the covariance matrix used in our χ^2 analysis follows from first principles. For a discussion about the angular power spectrum in light of finite counts see also [76].

Our analysis is based on the cross correlation angular power spectrum that is obtained from the measurements in some X-ray energy band i and the galaxy catalogue g (mostly 2MRS), and given by

$$C_{\ell i}^{\gamma, g} \equiv \langle a_{\ell m i}^{\gamma} (a_{\ell m}^g)^* \rangle \equiv \frac{1}{2\ell + 1} \sum_{m=-\ell}^{\ell} a_{\ell m i}^{\gamma} (a_{\ell m}^g)^* . \quad (\text{A.1})$$

Here, $a_{\ell m i}^{\gamma}$ ($a_{\ell m}^g$) are the modes of a decomposition of the *measured* X-ray sky map (galaxy catalogue) into spherical harmonics, and $\langle \dots \rangle$ denotes the usual average over m .

We are interested in the variations of $C_{\ell i}^{\gamma, g}$ over many measurements. In general, it holds that $\langle a_{\ell m i}^{\gamma} \rangle_r = \langle a_{\ell m}^g \rangle_r = 0$, where $\langle \dots \rangle_r$ is the average over cosmological realisations, and photon and galaxy shot noise. Furthermore, we find that

$$\langle a_{\ell m i}^{\gamma} (a_{\ell m j}^{\gamma})^* \rangle_r = \frac{4\pi}{N_{\gamma, i}} \langle I \rangle_i^2 \delta_{ij} + \sqrt{C_{\ell i}^{\gamma} C_{\ell j}^{\gamma}} , \quad (\text{A.2})$$

$$\langle a_{\ell m i}^{\gamma} (a_{\ell m}^g)^* \rangle_r = C_{\ell i}^{\gamma, g} , \quad (\text{A.3})$$

$$\langle a_{\ell m}^g (a_{\ell m}^g)^* \rangle_r = \frac{4\pi}{N_g} + C_{\ell}^g , \quad (\text{A.4})$$

where $N_{\gamma, i}$ is the number of photons in energy bin i , and $\langle I \rangle_i$ the corresponding full-sky averaged flux. The noise comes either from the finite number of photons in X-ray observations or the finite number of galaxies in the catalogue, and the cosmic variance contribution is a consequence of the stochasticity of structure formation. We assumed that the morphology of the signal changes only weakly between the relevant energy bins.

The covariance of the cross correlation angular power spectrum is then obtained as

$$\begin{aligned} (\Delta C_{\ell}^{\gamma, g})_{ij}^2 &\equiv \langle C_{\ell i}^{\gamma, g} C_{\ell j}^{\gamma, g} \rangle_r \\ &= \frac{1}{(2\ell + 1)^2} \sum_{m, m'=-\ell}^{\ell} \langle a_{\ell m i}^{\gamma} (a_{\ell m'}^g)^* a_{\ell m' j}^{\gamma} (a_{\ell m}^g)^* \rangle_r - \langle a_{\ell m i}^{\gamma} (a_{\ell m}^g)^* \rangle_r \langle a_{\ell m' j}^{\gamma} (a_{\ell m'}^g)^* \rangle_r \\ &= \frac{1}{(2\ell + 1)^2} \sum_{m=-\ell}^{\ell} \langle a_{\ell m i}^{\gamma} (a_{\ell m j}^{\gamma})^* \rangle_r \langle a_{\ell m}^g (a_{\ell m}^g)^* \rangle_r + \langle a_{\ell m i}^{\gamma} (a_{\ell m}^g)^* \rangle_r \langle a_{\ell m j}^{\gamma} (a_{\ell m}^g)^* \rangle_r \\ &= \frac{1}{(2\ell + 1)} \left[\left(\frac{4\pi}{N_{\gamma, i}} \langle I \rangle_i^2 \delta_{ij} + \sqrt{C_{\ell i}^{\gamma} C_{\ell j}^{\gamma}} \right) \left(\frac{4\pi}{N_g} + C_{\ell}^g \right) + C_{\ell i}^{\gamma, g} C_{\ell j}^{\gamma, g} \right] . \end{aligned} \quad (\text{A.5})$$

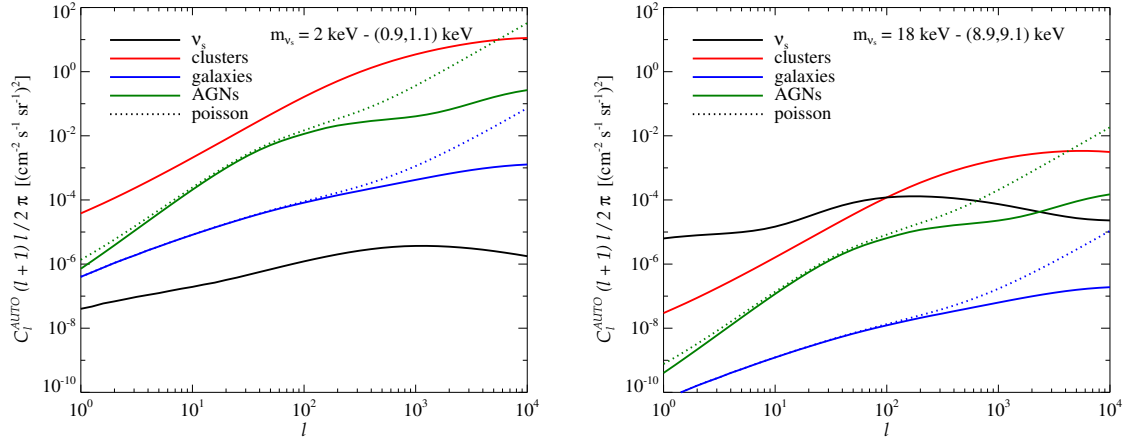


Figure 11. Left. Auto-correlation angular power spectrum of CXB due to sterile neutrino decays for $m_{\nu_s} = 2$ keV with a mixing angle corresponding to the constraint given by our baseline analysis as in Fig. 9, (unresolved) AGNs, (unresolved) galaxies, and (resolved and unresolved) clusters of galaxies in the 0.9 – 1.1 keV energy band. For AGNs and galaxies, both the correlation term (solid) and total including Poisson term (dotted) are shown. **Right.** The same but for $m_{\nu_s} = 18$ keV in the 8.9 – 9.1 keV energy band. We show both plots with the same scale for comparison, but note that the scale is different with respect to the left panel of Fig. 3.

The adopted Eq. (5.1) is then obtained after a rescaling of the photon power spectrum that inverts the (here energy-independent) effect of the finite angular resolution, e.g., $C_{\ell i}^\gamma \rightarrow C_{\ell i}^\gamma / W_\ell^2$.

B Auto- and cross-correlation power spectra

We show in Figs. 11 and 12 the auto-correlation and 2MRS cross-correlation power spectra in the 0.9 – 1.1 and 8.9 – 9.1 keV energy ranges corresponding to the sterile neutrino masses of $m_{\nu_s} = 2$ and 18 keV, respectively. In both cases, the sterile neutrino mixing angle is chosen to be just as from the constraints of our baseline analysis shown in Fig. 9. Our constraining power decrease dramatically moving toward higher energies, as clear both from Fig. 9 and from the error bars in the left panel of Fig. 12, due to the larger instrumental background.

References

- [1] G. Jungman, M. Kamionkowski, and K. Griest, *Supersymmetric dark matter*, *Phys.Rept.* **267** (1996) 195–373, [[hep-ph/9506380](#)].
- [2] G. Bertone, D. Hooper, and J. Silk, *Particle dark matter: Evidence, candidates and constraints*, *Phys. Rept.* **405** (2005) 279–390, [[hep-ph/0404175](#)].
- [3] S. Dodelson and L. M. Widrow, *Sterile-neutrinos as dark matter*, *Phys.Rev.Lett.* **72** (1994) 17–20, [[hep-ph/9303287](#)].
- [4] X.-D. Shi and G. M. Fuller, *A New dark matter candidate: Nonthermal sterile neutrinos*, *Phys.Rev.Lett.* **82** (1999) 2832–2835, [[astro-ph/9810076](#)].
- [5] A. Boyarsky, O. Ruchayskiy, and M. Shaposhnikov, *The role of sterile neutrinos in cosmology and astrophysics*, *Ann. Rev. Nucl. Part. Sci.* **59** (2009) 191–214, [[arXiv:0901.0011](#)].

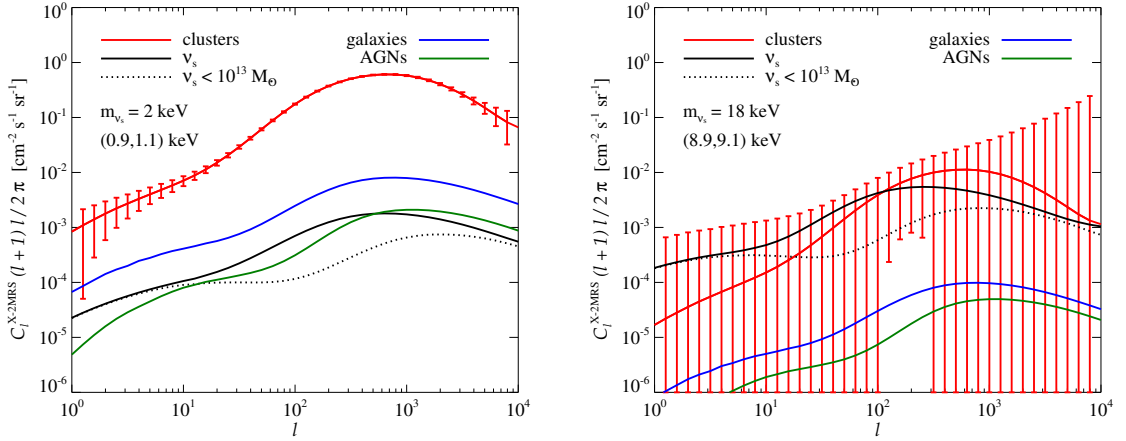


Figure 12. Cross correlation with 2MRS. We overlay to the cluster component the error bars, as $\Delta C_l / \sqrt{l/2}$, estimated from the diagonal part of the covariance matrix of Eq. 5.1. **Left.** Cross-correlation angular power spectrum of CXB due to sterile neutrino decays for $m_{\nu_s} = 2$ keV with a mixing angle corresponding to the constraint given by our baseline analysis as in Fig. 9, (unresolved) AGNs, (unresolved) galaxies, and (resolved and unresolved) clusters of galaxies in the 0.9 – 1.1 keV energy band. For sterile neutrinos, we also show the case when the integration upper mass limit is fixed to $M_{200}^{\nu, \text{lim}} \times h = 10^{13} M_\odot$. See main text for details. **Right.** The same but for $m_{\nu_s} = 18$ keV in the 8.9 – 9.1 keV energy band. We show both plots with the same scale for comparison, but note that the scale is different with respect to the left panel of Fig. 5.

- [6] A. Boyarsky, D. Iakubovskyi, and O. Ruchayskiy, *Next decade of sterile neutrino studies*, *Physics of the Dark Universe* **1** (Nov., 2012) 136–154, [[arXiv:1306.4954](#)].
- [7] M. R. Lovell, C. S. Frenk, V. R. Eke, A. Jenkins, L. Gao, and T. Theuns, *The properties of warm dark matter haloes*, *MNRAS* **439** (Mar., 2014) 300–317, [[arXiv:1308.1399](#)].
- [8] P. B. Pal and L. Wolfenstein, *Radiative Decays of Massive Neutrinos*, *Phys. Rev.* **D25** (1982) 766.
- [9] C. R. Watson, J. F. Beacom, H. Yüksel, and T. P. Walker, *Direct x-ray constraints on sterile neutrino warm dark matter*, *Phys. Rev. D* **74** (Aug., 2006) 033009, [[astro-ph/0605424](#)].
- [10] A. Boyarsky, D. Iakubovskyi, O. Ruchayskiy, and V. Savchenko, *Constraints on decaying dark matter from XMM-Newton observations of M31*, *MNRAS* **387** (July, 2008) 1361–1373, [[arXiv:0709.2301](#)].
- [11] A. Boyarsky, O. Ruchayskiy, D. Iakubovskyi, M. G. Walker, S. Riemer-Sørensen, and S. H. Hansen, *Searching for dark matter in X-rays: how to check the dark matter origin of a spectral feature*, *MNRAS* **407** (Sept., 2010) 1188–1202, [[arXiv:1001.0644](#)].
- [12] C. R. Watson, Z. Li, and N. K. Polley, *Constraining sterile neutrino warm dark matter with Chandra observations of the Andromeda galaxy*, *JCAP* **3** (Mar., 2012) 18, [[arXiv:1111.4217](#)].
- [13] S. Horiuchi, P. J. Humphrey, J. Oñorbe, K. N. Abazajian, M. Kaplinghat, and S. Garrison-Kimmel, *Sterile neutrino dark matter bounds from galaxies of the Local Group*, *Phys. Rev. D* **89** (Jan., 2014) 025017, [[arXiv:1311.0282](#)].
- [14] E. Figueroa-Feliciano, A. J. Anderson, D. Castro, D. C. Goldfinger, J. Rutherford, M. E. Eckart, R. L. Kelley, C. A. Kilbourne, D. McCammon, K. Morgan, F. S. Porter, and A. E. Szymkowiak, *Searching for keV Sterile Neutrino Dark Matter with X-ray Microcalorimeter Sounding Rockets*, *ArXiv e-prints* (June, 2015) [[arXiv:1506.05519](#)].

- [15] E. Bulbul, M. Markevitch, A. Foster, R. K. Smith, M. Loewenstein, et al., *Detection of An Unidentified Emission Line in the Stacked X-ray spectrum of Galaxy Clusters*, [arXiv:1402.2301](#).
- [16] A. Boyarsky, O. Ruchayskiy, D. Iakubovskiy, and J. Franse, *Unidentified Line in X-Ray Spectra of the Andromeda Galaxy and Perseus Galaxy Cluster*, *Phys. Rev. Letters* **113** (Dec., 2014) 251301, [[arXiv:1402.4119](#)].
- [17] A. Boyarsky, J. Franse, D. Iakubovskiy, and O. Ruchayskiy, *Checking the dark matter origin of 3.53 keV line with the Milky Way center*, *ArXiv e-prints* (Aug., 2014) [[arXiv:1408.2503](#)].
- [18] A. Boyarsky, J. Franse, D. Iakubovskiy, and O. Ruchayskiy, *Comment on the paper "Dark matter searches going bananas: the contribution of Potassium (and Chlorine) to the 3.5 keV line" by T. Jeltema and S. Profumo*, *ArXiv e-prints* (Aug., 2014) [[arXiv:1408.4388](#)].
- [19] E. Bulbul, M. Markevitch, A. R. Foster, R. K. Smith, M. Loewenstein, and S. W. Randall, *Comment on "Dark matter searches going bananas: the contribution of Potassium (and Chlorine) to the 3.5 keV line"*, *ArXiv e-prints* (Sept., 2014) [[arXiv:1409.4143](#)].
- [20] D. Iakubovskiy, E. Bulbul, A. R. Foster, D. Savchenko, and V. Sadova, *Testing the origin of 3.55 keV line in individual galaxy clusters observed with XMM-Newton*, *ArXiv e-prints* (Aug., 2015) [[arXiv:1508.05186](#)].
- [21] T. E. Jeltema and S. Profumo, *Discovery of a 3.5 keV line in the Galactic Center and a Critical Look at the Origin of the Line Across Astronomical Targets*, *ArXiv e-prints* (Aug., 2014) [[arXiv:1408.1699](#)].
- [22] D. Malyshev, A. Neronov, and D. Eckert, *Constraints on 3.55 keV line emission from stacked observations of dwarf spheroidal galaxies*, *Phys. Rev. D* **90** (Nov., 2014) 103506, [[arXiv:1408.3531](#)].
- [23] M. E. Anderson, E. Churazov, and J. N. Bregman, *Non-Detection of X-Ray Emission From Sterile Neutrinos in Stacked Galaxy Spectra*, *ArXiv e-prints* (Aug., 2014) [[arXiv:1408.4115](#)].
- [24] O. Urban, N. Werner, S. W. Allen, A. Simionescu, J. S. Kaastra, and L. E. Strigari, *A Suzaku Search for Dark Matter Emission Lines in the X-ray Brightest Galaxy Clusters*, *ArXiv e-prints* (Oct., 2014) [[arXiv:1411.0050](#)].
- [25] T. Jeltema and S. Profumo, *Reply to Two Comments on "Dark matter searches going bananas the contribution of Potassium (and Chlorine) to the 3.5 keV line"*, *ArXiv e-prints* (Nov., 2014) [[arXiv:1411.1759](#)].
- [26] E. Carlson, T. Jeltema, and S. Profumo, *Where do the 3.5 keV photons come from? A morphological study of the Galactic Center and of Perseus*, *JCAP* **2** (Feb., 2015) 9, [[arXiv:1411.1758](#)].
- [27] T. Tamura, R. Iizuka, Y. Maeda, K. Mitsuda, and N. Y. Yamasaki, *An X-ray spectroscopic search for dark matter in the Perseus cluster with Suzaku*, *Publications of the Astronomical Society of Japan* **67** (Apr., 2015) 23, [[arXiv:1412.1869](#)].
- [28] M. R. Lovell, G. Bertone, A. Boyarsky, A. Jenkins, and O. Ruchayskiy, *Decaying dark matter: the case for a deep X-ray observation of Draco*, *ArXiv e-prints* (Nov., 2014) [[arXiv:1411.0311](#)].
- [29] S. Camera, M. Fornasa, N. Fornengo, and M. Regis, *A Novel Approach in the Weakly Interacting Massive Particle Quest: Cross-correlation of Gamma-Ray Anisotropies and Cosmic Shear*, *ApJl* **771** (July, 2013) L5, [[arXiv:1212.5018](#)].
- [30] S. Ando, A. Benoit-Lévy, and E. Komatsu, *Mapping dark matter in the gamma-ray sky with galaxy catalogs*, *Phys. Rev. D* **90** (2014), no. 2 023514, [[arXiv:1312.4403](#)].
- [31] S. Camera, M. Fornasa, N. Fornengo, and M. Regis, *Tomographic-spectral approach for dark matter detection in the cross-correlation between cosmic shear and diffuse gamma-ray emission*,

- ArXiv e-prints* (Nov., 2014) [[arXiv:1411.4651](#)].
- [32] N. Fornengo and M. Regis, *Particle dark matter searches in the anisotropic sky*, *Frontiers in Physics* **2** (Feb., 2014) 6, [[arXiv:1312.4835](#)].
 - [33] M. Shirasaki, S. Horiuchi, and N. Yoshida, *Cross-Correlation of Cosmic Shear and Extragalactic Gamma-ray Background: Constraints on the Dark Matter Annihilation Cross-Section*, *Phys.Rev.* **D90** (2014), no. 6 063502, [[arXiv:1404.5503](#)].
 - [34] S. Ando, *Power spectrum tomography of dark matter annihilation with local galaxy distribution*, *JCAP* **1410** (2014), no. 10 061, [[arXiv:1407.8502](#)].
 - [35] J.-Q. Xia, A. Cuoco, E. Branchini, and M. Viel, *Tomography of the Fermi-LAT γ -Ray Diffuse Extragalactic Signal via Cross Correlations with Galaxy Catalogs*, *ApJs* **217** (Mar., 2015) 15, [[arXiv:1503.05918](#)].
 - [36] N. Fornengo, L. Perotto, M. Regis, and S. Camera, *Evidence of Cross-correlation between the CMB Lensing and the γ -Ray Sky*, *ApJL* **802** (Mar., 2015) L1, [[arXiv:1410.4997](#)].
 - [37] J.-Q. Xia, A. Cuoco, E. Branchini, and M. Viel, *Tomography of the Fermi-lat γ -ray Diffuse Extragalactic Signal via Cross Correlations With Galaxy Catalogs*, *Astrophys.J.Suppl.* **217** (2015), no. 1 15, [[arXiv:1503.05918](#)].
 - [38] M. Regis, J.-Q. Xia, A. Cuoco, E. Branchini, N. Fornengo, and M. Viel, *Particle Dark Matter Searches Outside the Local Group*, *Phys. Rev. Letters* **114** (June, 2015) 241301, [[arXiv:1503.05922](#)].
 - [39] A. Cuoco, J.-Q. Xia, M. Regis, E. Branchini, N. Fornengo, and M. Viel, *Dark matter searches in the gamma-ray extragalactic background via cross-correlations with galaxy catalogues*, *ArXiv e-prints* (June, 2015) [[arXiv:1506.01030](#)].
 - [40] M. Fornasa and M. A. Sanchez-Conde, *The nature of the Diffuse Gamma-Ray Background*, *ArXiv e-prints* (Feb., 2015) [[arXiv:1502.02866](#)].
 - [41] E. Sefusatti, G. Zaharijas, P. D. Serpico, D. Theurel, and M. Gustafsson, *Extragalactic gamma-ray signal from dark matter annihilation: an appraisal*, *MNRAS* **441** (2014), no. 3 1861–1878, [[arXiv:1401.2117](#)].
 - [42] W. Voges, B. Aschenbach, T. Boller, H. Bräuninger, U. Briel, W. Burkert, K. Dennerl, J. Englhauser, R. Gruber, F. Haberl, G. Hartner, G. Hasinger, M. Kürster, E. Pfeffermann, W. Pietsch, P. Predehl, C. Rosso, J. H. M. M. Schmitt, J. Trümper, and H. U. Zimmermann, *The ROSAT all-sky survey bright source catalogue*, *A&A* **349** (Sept., 1999) 389–405, [[astro-ph/9909315](#)].
 - [43] M. J. L. Turner, A. Abbey, M. Arnaud, M. Balasini, M. Barbera, E. Belsole, P. J. Bennie, J. P. Bernard, G. F. Bignami, M. Boer, U. Briel, I. Butler, C. Cara, C. Chabaud, R. Cole, A. Collura, M. Conte, A. Cros, M. Denby, P. Dhez, G. Di Coco, J. Dowson, P. Ferrando, S. Ghizzardi, F. Gianotti, C. V. Goodall, L. Gretton, R. G. Griffiths, O. Hainaut, J. F. Hochedez, A. D. Holland, E. Jourdain, E. Kendziorra, A. Lagostina, R. Laine, N. La Palombara, M. Lortholary, D. Lumb, P. Marty, S. Molendi, C. Pigot, E. Poindron, K. A. Pounds, J. N. Reeves, C. Reppin, R. Rothenflug, P. Salvetat, J. L. Sauvageot, D. Schmitt, S. Sembay, A. D. T. Short, J. Spragg, J. Stephen, L. Strüder, A. Tiengo, M. Trifoglio, J. Trümper, S. Vercellone, L. Vigroux, G. Villa, M. J. Ward, S. Whitehead, and E. Zonca, *The European Photon Imaging Camera on XMM-Newton: The MOS cameras : The MOS cameras*, *A&A* **365** (Jan., 2001) L27–L35, [[astro-ph/0011498](#)].
 - [44] M. C. Weisskopf, B. Brinkman, C. Canizares, G. Garmire, S. Murray, and L. P. Van Speybroeck, *An Overview of the Performance and Scientific Results from the Chandra X-Ray Observatory*, *The Publications of the Astronomical Society of the Pacific* **114** (Jan., 2002) 1–24, [[astro-ph/0110308](#)].

- [45] A. Merloni, P. Predehl, W. Becker, H. Böhringer, T. Boller, H. Brunner, M. Brusa, K. Dennerl, M. Freyberg, P. Friedrich, A. Georgakakis, F. Haberl, G. Hasinger, N. Meidinger, J. Mohr, K. Nandra, A. Rau, T. H. Reiprich, J. Robrade, M. Salvato, A. Santangelo, M. Sasaki, A. Schwobe, J. Wilms, and t. German eROSITA Consortium, *eROSITA Science Book: Mapping the Structure of the Energetic Universe*, *ArXiv:1209.3114* (Sept., 2012) [[arXiv:1209.3114](#)].
- [46] J. P. Huchra et al., *The 2MASS Redshift Survey—Description and Data Release*, *Astrophys. J. Suppl. Ser.* **199** (2012) 26, [[arXiv:1108.0669](#)].
- [47] S. Ando and E. Komatsu, *Constraints on the annihilation cross section of dark matter particles from anisotropies in the diffuse gamma-ray background measured with Fermi-LAT*, *Phys. Rev. D* **87** (2013), no. 12 123539, [[arXiv:1301.5901](#)].
- [48] A. C. Fabian and X. Barcons, *The origin of the X-ray background*, *Ann. Rev. Astron. Astrophys.* **30** (1992) 429–456.
- [49] E. Treister and C. M. Urry, *The Evolution of Obscuration in AGN*, *Astrophys. J.* **652** (2006) L79–L82, [[astro-ph/0610525](#)].
- [50] R. Gilli, G. Risaliti, and M. Salvati, *Beyond the standard model for the cosmic x-ray background*, *Astron. Astrophys.* **347** (1999) 424, [[astro-ph/9904422](#)].
- [51] B. Lehmer, Y. Xue, W. Brandt, D. Alexander, F. Bauer, et al., *The 4 Ms Chandra Deep Field-South Number Counts Apportioned by Source Class: Pervasive Active Galactic Nuclei and the Ascent of Normal Galaxies*, *Astrophys. J.* **752** (2012) 46, [[arXiv:1204.1977](#)].
- [52] J. Aird, K. Nandra, E. S. Laird, A. Georgakakis, M. L. N. Ashby, P. Barmby, A. L. Coil, J.-S. Huang, A. M. Koekemoer, C. C. Steidel, and C. N. A. Willmer, *The evolution of the hard X-ray luminosity function of AGN*, *MNRAS* **401** (2010) 2531–2551, [[arXiv:0910.1141](#)].
- [53] P. Tozzi, R. Gilli, V. Mainieri, C. Norman, G. Risaliti, et al., *X-ray spectral properties of agn in the chandra deep field south*, *Astron. Astrophys.* **451** (2006) 457, [[astro-ph/0602127](#)].
- [54] A. Ptak, B. Mobasher, A. Hornschemeier, F. Bauer, and C. Norman, *X-Ray Luminosity Functions of Normal Galaxies in the Great Observatories Origins Deep Survey*, *Astrophys. J.* **667** (2007) 826–858.
- [55] M. Young, W. Brandt, Y. Xue, M. Paolillo, D. Alexander, et al., *Variability Selected Low-Luminosity Active Galactic Nuclei in the 4 Ms Chandra Deep Field-South*, *Astrophys. J.* **748** (2012) 124, [[arXiv:1201.4391](#)].
- [56] G. M. Voit, *Tracing cosmic evolution with clusters of galaxies*, *Reviews of Modern Physics* **77** (Apr., 2005) 207–258, [[astro-ph/0410173](#)].
- [57] R. Piffaretti, M. Arnaud, G. W. Pratt, E. Pointecouteau, and J.-B. Melin, *The MCXC: a meta-catalogue of x-ray detected clusters of galaxies*, *A&A* **534** (Oct., 2011) A109, [[arXiv:1007.1916](#)].
- [58] C. L. Sarazin, *X-ray emission from clusters of galaxies*. Cambridge Astrophysics Series, Cambridge: Cambridge University Press, 1988, 1988.
- [59] J. Tinker, A. V. Kravtsov, A. Klypin, K. Abazajian, M. Warren, G. Yepes, S. Gottlöber, and D. E. Holz, *Toward a Halo Mass Function for Precision Cosmology: The Limits of Universality*, *Astrophys. J.* **688** (Dec., 2008) 709–728, [[arXiv:0803.2706](#)].
- [60] S. G. Murray, C. Power, and A. S. G. Robotham, *HMFcalc: An online tool for calculating dark matter halo mass functions*, *Astronomy and Computing* **3** (Nov., 2013) 23–34, [[arXiv:1306.6721](#)].
- [61] F. Zandanel, C. Pfrommer, and F. Prada, *A phenomenological model for the intracluster medium that matches X-ray and Sunyaev-Zel’dovich observations*, *MNRAS* **438** (Feb., 2014)

- 116–123, [[arXiv:1311.4793](#)].
- [62] W. Hu and A. V. Kravtsov, *Sample Variance Considerations for Cluster Surveys*, *Astrophys.J.* **584** (Feb., 2003) 702–715, [[astro-ph/0203169](#)].
 - [63] S. Ando, E. Komatsu, T. Narumoto, and T. Totani, *Dark matter annihilation or unresolved astrophysical sources? Anisotropy probe of the origin of cosmic gamma-ray background*, *Phys. Rev. D* **75** (2007) 063519, [[astro-ph/0612467](#)].
 - [64] A. Cooray and R. K. Sheth, *Halo models of large scale structure*, *Phys. Rept.* **372** (2002) 1–129, [[astro-ph/0206508](#)].
 - [65] J. L. Tinker, B. E. Robertson, A. V. Kravtsov, A. Klypin, M. S. Warren, et al., *The Large Scale Bias of Dark Matter Halos: Numerical Calibration and Model Tests*, *Astrophys.J.* **724** (2010) 878–886, [[arXiv:1001.3162](#)].
 - [66] M. Viel, G. D. Becker, J. S. Bolton, and M. G. Haehnelt, *Warm dark matter as a solution to the small scale crisis: New constraints from high redshift Lyman- forest data*, *Phys. Rev. D* **88** (2013) 043502, [[arXiv:1306.2314](#)].
 - [67] S. Bose, W. A. Hellwing, C. S. Frenk, A. Jenkins, M. R. Lovell, J. C. Helly, and B. Li, *The COpernicus COmplexio: Statistical Properties of Warm Dark Matter Haloes*, *ArXiv e-prints* (July, 2015) [[arXiv:1507.01998](#)].
 - [68] J. F. Navarro, C. S. Frenk, and S. D. M. White, *A Universal Density Profile from Hierarchical Clustering*, *Astrophys.J.* **490** (Dec., 1997) 493–508, [[astro-ph/9611107](#)].
 - [69] F. Prada, A. A. Klypin, A. J. Cuesta, J. E. Betancort-Rijo, and J. Primack, *Halo concentrations in the standard Λ cold dark matter cosmology*, *MNRAS* **423** (July, 2012) 3018–3030, [[arXiv:1104.5130](#)].
 - [70] V. Allevato, A. Finoguenov, N. Cappelluti, T. Miyaji, G. Hasinger, et al., *The XMM-Newton Wide field survey in the COSMOS field: redshift evolution of AGN bias and subdominant role of mergers in triggering moderate luminosity AGN at redshift up to 2.2*, *Astrophys.J.* **736** (2011) 99, [[arXiv:1105.0520](#)].
 - [71] N. Cappelluti, P. Ranalli, M. Roncarelli, P. Arevalo, G. Z. A. Comastri, et al., *The nature of the unresolved extragalactic soft CXB*, *MNRAS*. **427** (2012) 651, [[arXiv:1208.4105](#)].
 - [72] T. Jarrett, T. Chester, R. Cutri, S. Schneider, J. L. Rosenberg, et al., *2mass extended sources in the zone of avoidance*, *Astron. J.* **120** (2000) 298–313, [[astro-ph/0005017](#)].
 - [73] J.-Q. Xia, A. Cuoco, E. Branchini, M. Fornasa, and M. Viel, *A cross-correlation study of the Fermi-LAT γ -ray diffuse extragalactic signal*, *Mon. Not. Roy. Astron. Soc.* **416** (2011) 2247–2264, [[arXiv:1103.4861](#)].
 - [74] C. Weniger et al. in preparation.
 - [75] S. Campbell et al. in preparation.
 - [76] S. S. Campbell, *Angular Power Spectra with Finite Counts*, *MNRAS* **448** (2015), no. 3 2854–2878, [[arXiv:1411.4031](#)].